sciendo

DOI 10.2478/ama-2024-0046

acta mechanica et automatica, vol.18 no.3 (2024)

EFFECT OF PORE ARCHITECTURE OF 3D PRINTED OPEN POROSITY CELLULAR STRUCTURES ON THEIR RESISTANCE TO MECHANICAL LOADING: PART I – EXPERIMENTAL STUDIES

Monika BERNACKA*/, Mehmet ALADAG*, Adrian DUBICKI*, Izabela ZGŁOBICKA***

*Faculty of Mechanical Engineering, Bialystok University of Technology, Wiejska 45C, 15-351 Bialystok
**Technology Applied Sp. z o.o., Wiejska 42/3, 15-509 Sobolewo, Poland

monika.bernacka@sd.pb.edu.pl, mehmet.aladag@sd.pb.edu.pl, a.dubicki@pb.edu.pl, i.zglobicka@pb.edu.pl

received 20 June 2023, revised 1 February 2024, accepted 27 February 2024

Abstract: The development of additive manufacturing (AM) techniques has sparked interest in porous structures that can be customized in terms of size, shape, and arrangement of pores. Porous lattice structure (LS, called also lattice struct) offer superior specific stiffness and strength, making them ideal components for lightweight products with energy absorption and heat transfer capabilities. They find applications in industries such as aerospace, aeronautics, automotive, and bone ingrowth applications. One of the main advantages of additive manufacturing is the freedom of design, control over geometry and architecture, cost and time savings, waste reduction, and product customization. However, the designation of appropriate struct/pore geometry to achieve the desired properties and structure remains a challenge. In this part of the study, five lattice structs with various pore sizes, with two volume fractions for each, and shapes (ellipsoidal, helical, X-shape, trapezoidal, and triangular) were designed and manufactured using selective laser sintering (SLS) additive manufacturing technology. Mechanical properties were tested through uniaxial compression, and the apparent stress-strain curves were analyzed. The results showed that the compression tests revealed both monotonic and non-monotonic stress-strain curves, indicating different compression behaviors among the structures. The helical structure exhibited the highest resistance to compression, while other structures showed similarities in their mechanical properties. In Part II of this study provides a comprehensive analysis of these findings, emphasizing the potential of purpose-designed porous structures for various engineering applications.

Key words: Additive manufacturing (AM), porous structures, lattice structs, selective laser sintering, mechanical properties

1. INTRODUCTION

Development of additive manufacturing (AM) (also known as 3D printing) techniques stimulated interest in porous structures which can be designed in terms of size, shape, and arrangement of pores. Of special importance are porous structures composed of repeating cellular units - typically generated by a periodic arrangement of beams/struts forming a three-dimensional framework. Superior specific stiffness and strength of lattice structures (LS, called lattice struct) make them ideal components of lightweight products, which may have the capacity for energy absorption and efficient heat transfer. They are thus widely used in industries such as aerospace, aeronautic and automotive. Their low mass, tunable elastic modulus, and porous nature make them suitable for bone ingrowth applications (1–3). Some of the key advantages of these methods over standard techniques of fabrication of porous materials are design freedom, full control of geometry and architecture, time and cost saving, waste reduction, and the possibility of product customization. Currently, available 3D printing devices allow for the fabrication of products from materials such as metal, ceramics, polymers, and composites. The challenge remains the selection of appropriate technology and process parameters assuring the required properties and structure of printed artifacts (4–7).

Selective laser sintering (SLS) is one of the common methods of additive manufacturing. The most commonly employed material in SLS printing technology offered by EOS is Polyamide (PA-2200). The other materials include TPU 1301, PA-3200 GF (blends polyamide with glass fiber), Alumide (based on PA12 with aluminum), and PA 2210 FR. Its distinct characteristic is that particles of powdered substrate are sintered by a laser beam with no formation of liquid phase. This allows for the fabrication of material-wise highly uniform structures of highly complex architecture (8). Ultra-lightweight elements of controlled porosity can be printed by SLS, which are the subject of the current paper, in which we focus on attention on fine-tuning mechanical properties of lattice-type porous structure by adjusting the size, shape, and arrangement of pores.

Numerous studies have been conducted by researchers to explore the design and fabrication of porous structures. Dong et al (9) made a wide review to collect the affecting parameters on the fabrication of LS. Mantachie et al (10) conducted a research study focusing on the mechanical response of Selective Laser Melting (SLM) lattice structs. Their work aimed to address the lack of an overarching analysis of the mechanical properties of the particular lattice structures. Through a comprehensive review of experimental data, Mantachie provided valuable insights into the design, fabrication, and performance of SLM lattice structs, encompassing their mechanical, electrical, thermal, and acoustic properties. The studies can be replicated with the various researches (11–14). Some of these studies are focused on limitations (capacity) fabrication of porous structures. Yuan et al. (15) prepared a review of additive manufacturing of polymeric composites from material

processing to structural design. It may be also a comprehensive guide to the stakeholders who want to utilize or develop an AM process for polymeric composites. Supporting this study, Hossain et al. (16) addressed the limitations of typical periodic unit cells in porous structures created through laser powder bed fusion (PBF) additive manufacturing. They introduced modifications to create isotropic stochastic porous structures, and identified a remaining limitation in the standard deviation of the elastic modulus values. While the structures showed an improved isotropy and potential for lightweighting and biomaterial applications, further refinement is needed to enhance consistency in their mechanical performance. Both studies contribute valuable knowledge and fill existing gaps in the field. Efforts have been made by researchers to overcome these limitations by refining the processing parameters and improving the porous geometry as well as the mechanical characteristics. This represents an improvement in the thermal and mechanical characteristics of porous structures. To date, several studies have been conducted in this area. Han et al. (17) conducted a thorough review of LS, encompassing their properties, applications, and fabrication methods. They categorized lattice structures as uniform and non-uniform and examine different design approaches, including geometric unit cell-based, mathematical algorithm-generated, and topology optimization methods. The authors also investigated gradient and topology optimization techniques for non-uniform lattice structs and offer insights into the future development of this field. Supporting this research, several studies were conducted to optimize/characterize the structures (18–23). In particular, the compressive behavior of the lattice structs (24–26).

In this study, we designed lattice structures (LS) with two different pore sizes, 1.4 mm, and 1.9 mm, and incorporated five different pore shapes; ellipsoidal, helix, x-shapes, trapezoid, triangle in terms of unit cells. Subsequently, these designs were fabricated using SLS printing technology. To elucidate the impact of pore shape on mechanical properties, compression tests were conducted for each structure.

Initially, the density of the fabricated structures was computed. Following this, a microscopic examination was conducted to identify any manufacturing anomalies. Subsequently, uniaxial compression was applied to the structures. Notably, characteristic features of the apparent stress-strain curves derived from the compression tests were analyzed for each structure. Finally, the applied load, in tandem with the resulting strains, was quantified as a function of their relative density. The results were detailly discussed.

2. MATERIALS AND METHODS

2.1. Modelling the Lattices

Five types of 3D lattices with different geometry of the pores have been designed. SolidWorks was employed to create these lattices structures. The types can be described as having cell units based on and illustrated in **Fig 1**:

- ellipsoidal,
- helix,
- x-shape,
- trapezoid,
- triangle.

Each type specimens were printed in the form of cubes 30 x 30 x 30 mm. Two volume fractions for each structure were obtained under conditions of constant size of the pores of 1.4 and 1.9 mm. The corresponding specimens for each structure type are designated as HP (high porosity) and LP (low porosity), respectively.

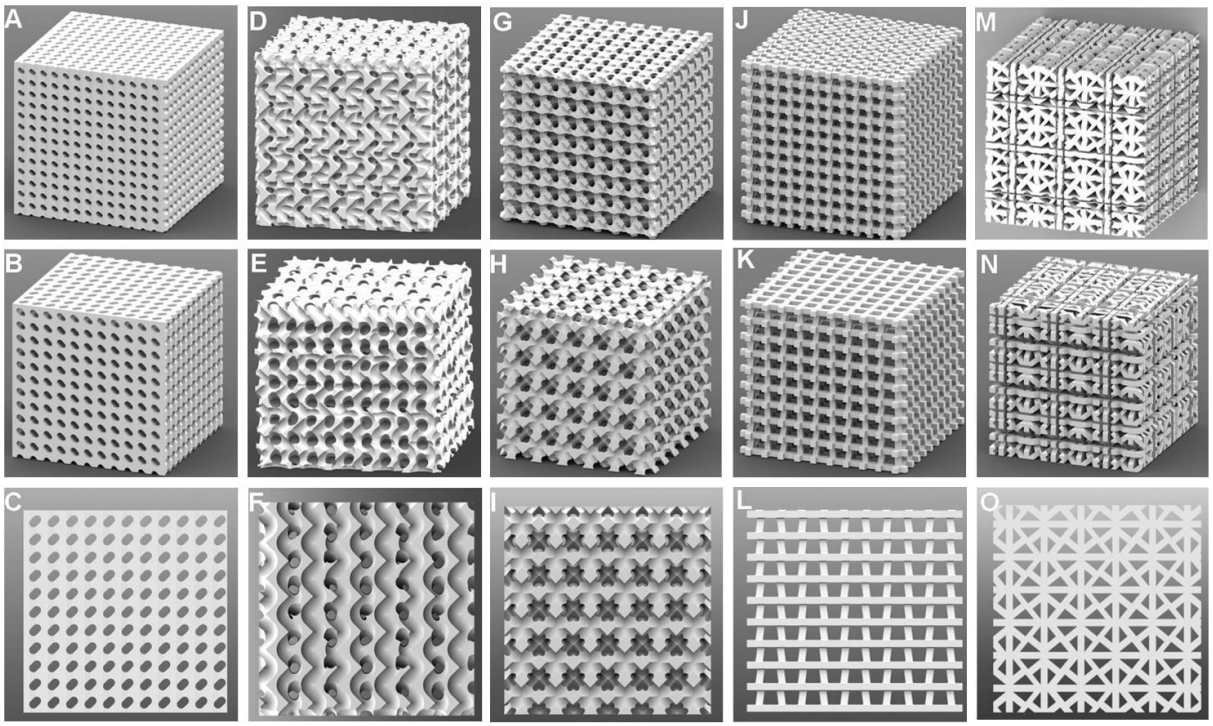

Fig 1. Designed CAD models of lattice structs: (A-C) ellipsoidal , (D-F) helical, (G-I) X-shape, (J-L) trapezoidal, (M-O) triangular, LP (A, D, G, J, M), HP (B, E, H, K, N), representative cross sections (C, F, I, L, O)

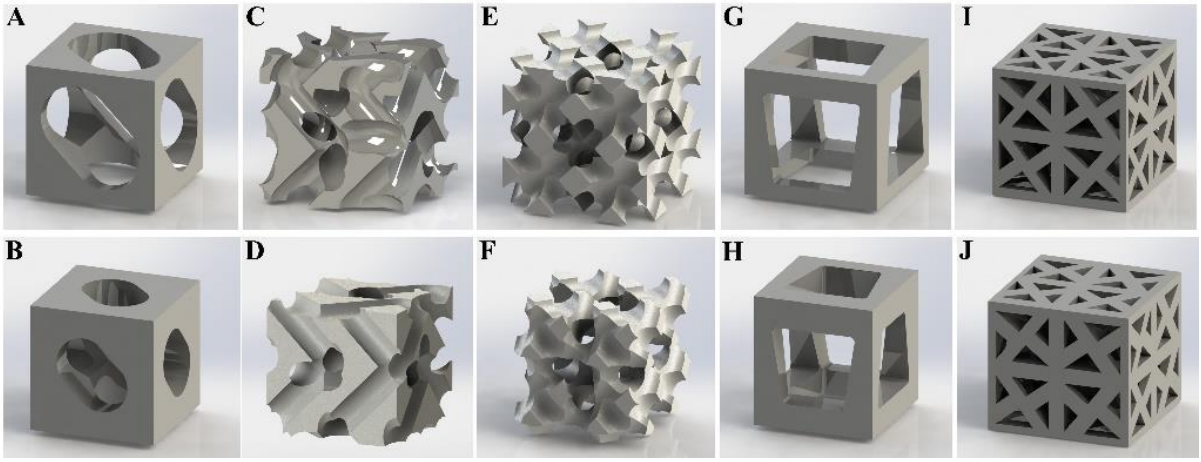

Fig 2. Single cells of lattice structs: (A-B) ellipsoidal , (C-D) helical, (E-F) X-shape, (G-H) trapezoidal, (I-J) triangular, LP (A, C, E, G, I), HP (B, D, F, H, J)

2.2. Fabrication

Lattice structs have been fabricated with SLS 3D printer EOS P395 (EOS GmbH Electro Optical Systems, Germany). The structures were positioned with the same orientation on the bed. The schematical illustration of the printing process is given in Fig 3. Printing process parameters, given in Tab. 1, were kept constant.

Polyamide (PA 2200), used in the present study is one of the most commonly employed material in Selective Laser Sintering (SLS) printing technology offered by EOS. This synthetic thermoplastic polymer has a high biocompatibility, flexibility, hygroscopicity, good chemical resistance as well as high strength and hardness. Selected mechanical properties of polyamide are listed in Tab. 2.

Tab. 1. Parameters of the printing process

Parameters		Unit	Value
Proportions of the virgin/recycled powder		%	50/50
Laser power		W	30
Process temperature		°C	175.5
Temperature of the working chamber		°C	130
Layer thickness		mm	0.12
Material shrinkage	along the X axis	%	3.23
	along the Y axis		3.24
	along the Z axis (0)		2.55
	along the Z axis (600)		1.4

Tab. 2. Mechanical properties of PA 2200

Mechanical properties	Value	Unit
Density	930	kg/m^3
Tensile strength	48	MPa
Tensile Modulus	1650	MPa
Strain at break	18	%
Melting temperature (20°C/min)	176	ºC
Shore D hardness	75	—
Powder size	60	µm

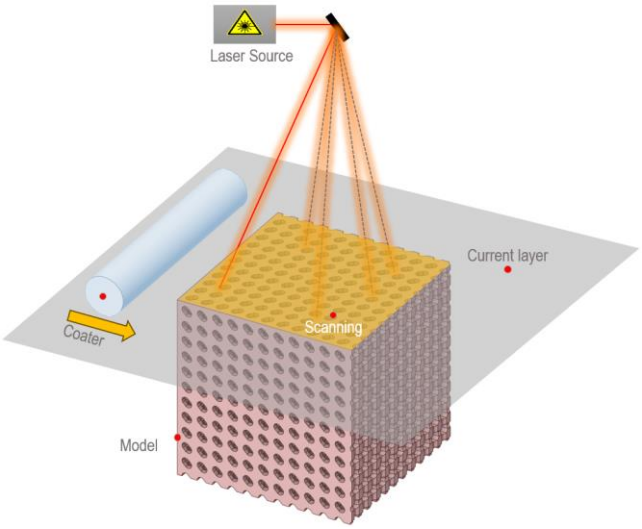

Fig 3. The schematic illustration of the printing process

2.3. Compression Test

The compression test was conducted utilizing 322 MTS Load Unit testing machine, incorporating a video extensometer, Aramis 3D (4M), to capture strain localization precisely. The lattice structures were positioned on the platform of the testing machine, and deformation was initiated by imparting a motion of 0.05 mm/sec along the -Y direction. A schematic illustration of the compression test is presented in Fig. 4. Data acquisition during the test was performed by the video extensometer, recording at a rate of 5 images per second to ensure accurate deformation measurement.

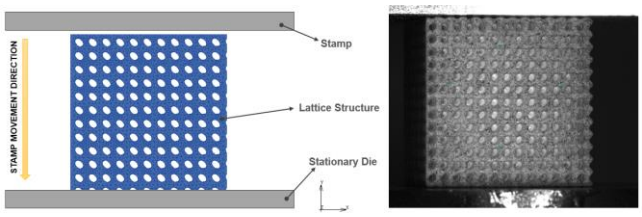

Fig. 4. Schematical illustration of the compression test and a view from the Aramis video extensometer.

3. RESULTS AND DISCUSSION

Surface quality of printed specimens was verified with digital microscope (Tagarno Magnus Prestige FHD). Single, un-sintered powder particles were observed between the lattice struts (indicated with arrows in Fig. 5). Mathematical statistical tools were not used due to their very small numbers. It has been assumed that these rarely found printing flaws have negligible effect under conditions of compression tests.The arithmetical value of 3 measurements was taken as the tests results.

The mass of the printed structures, apparent density and porosity are listed in Tab. 3 and shown in Fig. 6. The values of density and porosity of the manufactured samples in Tab.3 was based on the Archimedes law. The highest density/lowest porosity features X-shape LP – 1.03 g/mm3. The HP trapezoidal has the lowest apparent density of 0.647g/ mm3.

As can be seen from Fig. 6, experimental porosity of the printed specimens ranges from 50.46 to 82% and theoretical porosity from 45 to 72%. Experimental porosities of the printed structures have been compared with the theoretical values obtained from CAD modelling – see Fig. 6. It can be concluded that experimental values were higher than predicted from CAD data, apart from helical. Higher than predicted porosity of print-outs can be explained in terms of the effect of struts surface roughness.

Forces applied in compression tests have been analyzed in terms of apparent stress, defined as force divided by cube surface area, as function of strain, defined as reduction in cube height. The stress and strain curves for each structure were plotted in Fig. 7. The solid curves present for LP variants and the dashed for HP ones.

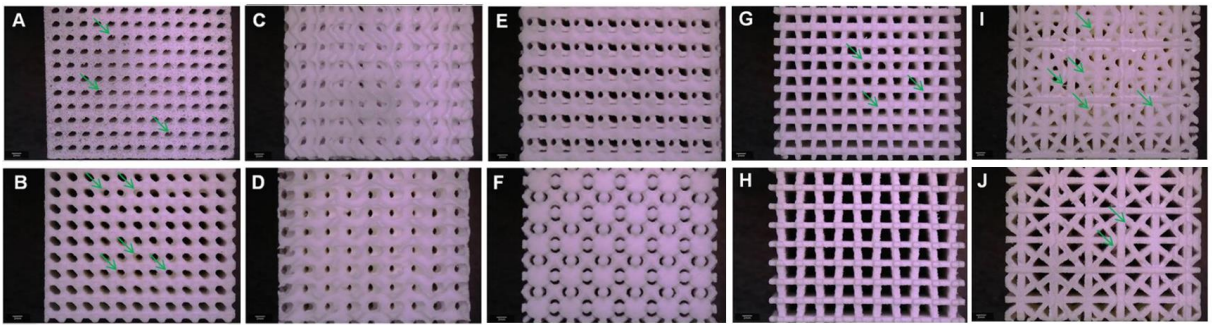

Fig. 5: Digital microscope images of manufactured structures: (A-B) ellipsoidal, (C-D) helical, (E-F) X-shape, (G-H) trapezoidal, (I-J) triangular, where: LP (A, C, E, G, I), HP (B, D, F, H, J); green arrows: single, un-sintered powder particles

Tab. 3. The average mass, density and porosity of the manufactured samples

Structure		Mass [g]	Density [g/mm^3]	Porosity [%]
Type of structure	Porosity			
Ellipsoidal	LP	11.23 ± 0.01	0.777	59.15
	HP	9.22 ± 0.14	0.750	62.90
Helical	LP	13.11 ± 0.68	1.03	66.24
	HP	12.33 ± 0.22	0.879	66.71
X-shape	LP	8.77 ± 0.20	0.819	50.46
	HP	8.43 ± 0.06	0.799	51.57
Trapezoidal	LP	6.4 ± 0.22	0.675	73.32
	HP	4.4 ± 0.07	0.647	82.82
Triangular	LP	10.09 ± 0.36	0.828	60.35
	HP	7.33 ± 0.10	0.704	65.99

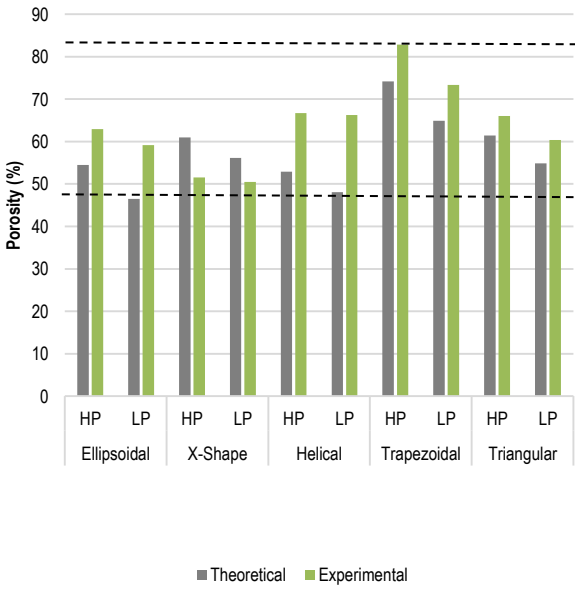

Fig. 6. Porosities of the examined structures

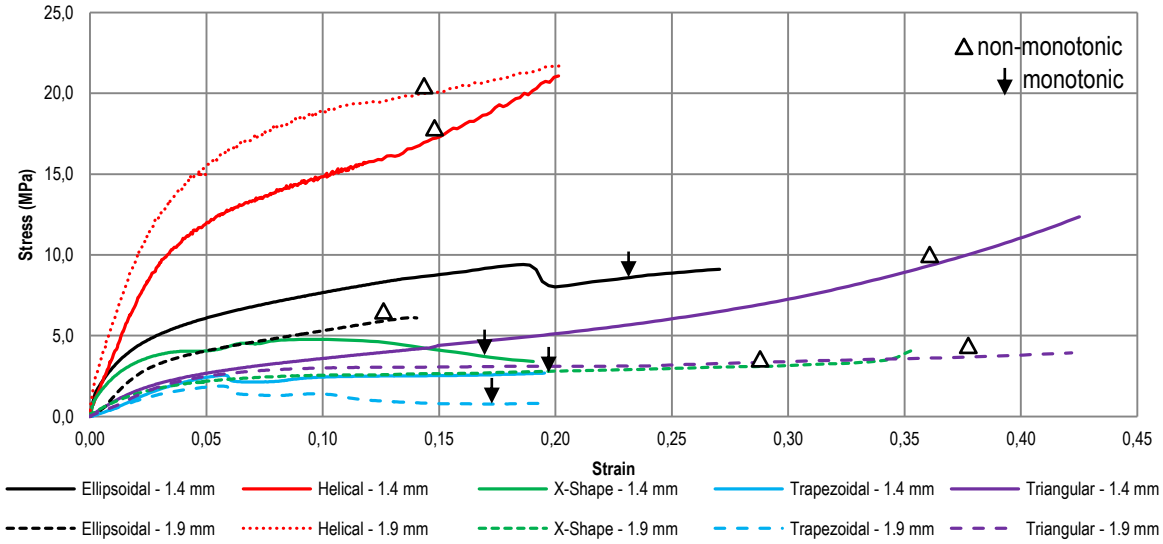

Fig. 7. Stress-strain curves for the samples of the investigated structures

Two types of curves can be distinguished in Fig. 7: (a) monotonic (arrows) and (b) non-monotonic (triangle). To elucidate differences in the compression behavior of various structures, analyses were carried out of apparent stresses at 5 and 15% of apparent strain. The stress values were normalized by the density of a given samples. The results are presented in Tab. 4 and

Tab. 5, for monotonic and non-monotonic curves.

It can be concluded that the tested structures show comparable mechanical properties to previously tested structures with similar parameters, however different unit cells made by using SLS printing technology. Change in pore size and architecture contributed to a decrease/increase in the analyzed mechanical values. The experimental Young's modulus of lattice structs in previous studies ranged from 102.63 to 335.14 MPa. The yield strength of lattice structs ranges from 2.07 to 13.73 MPa. The structures examined in the article are characterized by a Young's modulus of 47.54 -544.12 MPa and a yield strength of 0.935-9.95 MPa (27). Han et al. (28) developed a graded structure through. They established a mathematical correlation between graded porosity and compressive properties. By adjusting the graded volume fraction, the elastic modulus and yield strength of the structures can be customized within the range of 0.28–0.59 GPa and 3.79–17.75 MPa, respectively.

Tab. 4. Normalized values of forces for monotonic parts

Structure	Porosity	$F_{5\%}$ $[\frac{kN}{g/mm^3}]$	$F_{15\%}$ $[\frac{kN}{g/mm^3}]$	Young's modulus $[\frac{GPa}{g/mm^3}]$	Initial stiffness $[\frac{1}{g/mm^3}]$
Ellipsoidal	LP	9.27	12.32	0.72	1413.71
	HP	5.2	-	0.47	463.28
Helical	LP	14.18	19.58	1.16	2395.3
	HP	16.49	22.08	1.44	2025.1
X-shape	LP	5.19	5.58	0.56	1109.86
	HP	2.75	3.17	0.23	299.73
Triangular	LP	3.31	5.21	0.25	339.44
	HP	2.83	4.08	0.38	235.56

Tab. 5. Normalized values of forces for non-monotonic parts

Structure	Porosity	F_{max} $[\frac{kN}{g/mm^3}]$	F_{min} $[\frac{kN}{g/mm^3}]$	$F_{5\%}$ $[\frac{kN}{g/mm^3}]$	$F_{15\%}$ $[\frac{kN}{g/mm^3}]$	Initial stiffness $[\frac{1}{g/mm^3}]$
Trapezoidal	LP	4.22	1.79	3.32	2.00	633.66
	HP	2.55	0.87	2.22	1.07	496.31

Tab. 6. Values of forces for all tested structure

Structure	Porosity	Young's modulus [MPa]	Yield strength [MPa]
Ellipsoidal	LP	492,23	3,05
	HP	126,09	2,63
Helical	LP	352,92	9,09
	HP	544,12	9,95
X-shape	LP	306,42	2,422
	HP	70,176	1,57
Trapezoidal	LP	56,247	2,066
	HP	47,536	1,368
Triangular	LP	83,972	1,856
	HP	59,64	0,935

The highest value of the force for 5% deformation was obtained for the helical with LP porosity - 16.49 kN/(g/mm^3). The non-monotonic structure helical and trapezoidal have similar values of the force F_{max}. The highest values of the F_{max} were obtained for LP X-shape, equal to 6.77 kN/(g/mm^3). Additionally, for non-monotonic structures, the minimal force F_{min} was calculated. HP trapezoidal has the highest value of this parameter, equal to 0.87 kN/(g/mm^3).

Structures ellipsoidal, X-shape, trapezoidal and triangular were characterized by a high similarity of the obtained values of the initial stiffness (see in Fig. 8). The highest values of the initial stiffness were obtained for monotonic LP helical equal to 2395.3 (1/g/mm^3). In all specimens the initial stiffness dropped with the increasing porosity.

By analyzing the values of normalized forces obtained for 15% deformation a high similarity of the obtained values for porous X-shape and trapezoidal was observed. The highest value of the force for 15% deformation was measured for LP helical, equal to 22.08 kN/(g/mm^3) (see in Fig. 9). All obtained values of compression force under 15% of strain were plotted in Fig. 9. This plot allows to notice distinct compression resistance of helical. Also, it can be noted that unlike in the case of structures X-shape, trapezoidal, triangular, higher compression force has been measured for HP case.

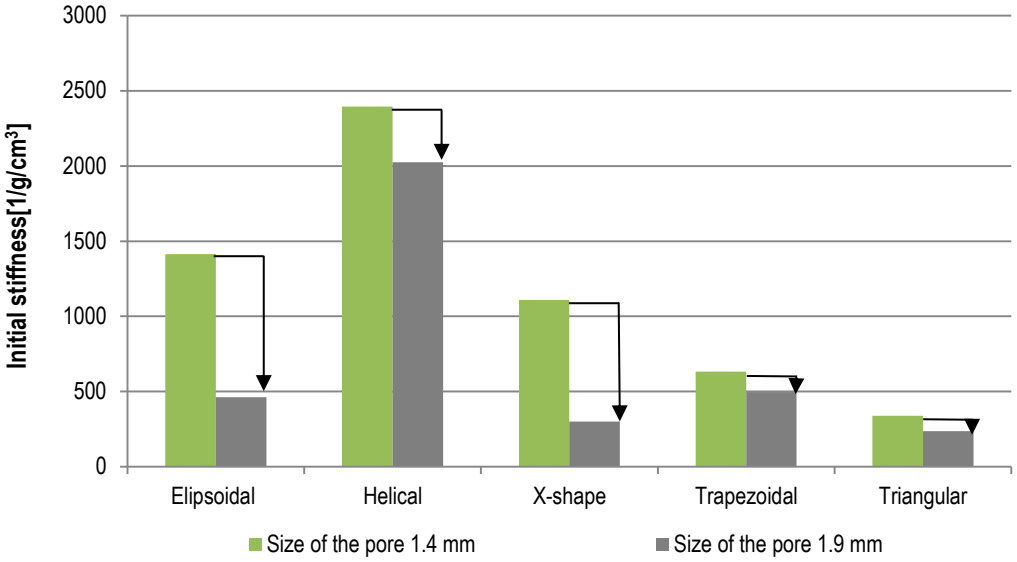

Fig. 8. Initial stiffness for structure with size of the pore 1.4 and 1.9 mm; black arrows: increase/decrease in values

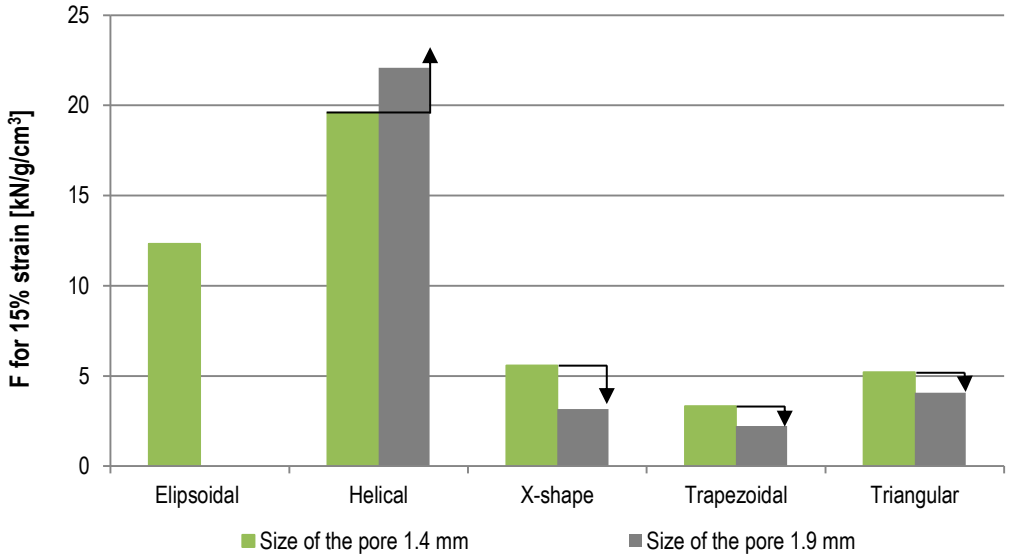

Fig. 9. F for 15% strain for structure with size of the pore 1.4 and 1.9 mm; black arrows: increase/decrease in values

In Tab. 7 - 16, the strains as a result of deformation in both direction , X and Y, are given for each structure. To measure the displacement, the two points were selected in X and Y direction and the distance between these points is given in L_{iy} and L_{ix} columns for unloaded condition, L_{fy} and L_{fx} for after 10% of deformation. For each structure, the displacement values in both the Y and X directions and the corresponding stresses give information about their mechanical behavior. Under 0% strain, the measurements represent the initial configurations of the structures and show no deformation. In contrast, under 10% strain, the displacement values show the response of the shapes to external forces and show the extent of deformation, with strain values measuring this change. It can be noted that all structures showcase a positive Poisson's ratio in response to deformation. Under a 10% strain, the strains in the X-direction remain uniform among the ellipsoidal, X-shaped, trapezoidal, and triangular structures, each registering a 1% strain. However, the helical structure differs from other structures, showing a difference of 1% between LP and HP configurations. Specifically, the LP helical structure shows a 2% strain, while the HP exhibits a 3% strain. As previously noted, in this comparative analysis table, the helical structure carried a remarkable load of approximately 17 kN compared to other structures.

Tab. 7. Results of displacement measurements for ellipsoidal – 0% strain

Ellipsoidal	Force [N]	L_{iy} [mm]	Strain Y	L_{ix} [mm]	Strain X
LP	0	17.75	0	19.91	0
HP		13.64		20.59	

Tab. 8. Results of displacement measurements for ellipsoidal – 10% strain

Ellipsoidal	Force [N]	L_{fy} [mm]	Strain Y	L_{fx} [mm]	Strain X
LP	8825.38	15.96	0.1	20.22	0.01
HP	4637.57	12.28		20.75	

Tab. 9. Results of displacement measurements for helical – 0% strain

Helical	Force [N]	L_{iy} [mm]	Strain Y	L_{ix} [mm]	Strain X
LP	0	18.21	0	17.69	0
HP		14.76		19.97	

Tab. 10. Results of displacement measurements for helical – 10% strain

Helical	Force [N]	L_{fy} [mm]	Strain Y	L_{fx} [mm]	Strain X
LP	17482.67	16.4	0.1	18.01	0.02
HP	18034.79	13.25		20.65	0.03

Tab. 11. Results of displacement measurements for X-shape – 0% strain

X-Shape	Force [N]	L_{iy} [mm]	Strain Y	L_{ix} [mm]	Strain X
LP	0	17.85	0	14.02	0
HP		24.49		24.89	

Tab. 12. Results of displacement measurements for X-shape – 10% strain

X-Shape	Force [N]	L_{fy} [mm]	Strain Y	L_{fx} [mm]	Strain X
LP	5537.68	16.03	0.1	14.09	0.01
HP	2517.55	22.07		25.24	

Tab. 13. Results of displacement measurements for trapezoidal – 0% strain

Trapezoidal	Force [N]	L_{iy} [mm]	Strain Y	L_{ix} [mm]	Strain X
LP	0	27.22	0	22.6	0
HP		21.22		20.54	

Tab. 14. Results of displacement measurements for trapezoidal – 10% strain

Trapezoidal	Force [N]	L_{fy} [mm]	Strain Y	L_{fx} [mm]	Strain X
LP	3931.84	24.49	0.1	22.72	0.01
HP	868.04	19.12		20.69	

Tab. 15. Results of displacement measurements for triangular – 0% strain

Triangular	Force [N]	L_{iy} [mm]	Strain Y	L_{ix} [mm]	Strain X
LP	0	18.44	0	20.77	0
HP		20.79		20.87	

Tab. 16. Results of displacement measurements for triangular – 10% strain

Triangular	Force [N]	L_{fy} [mm]	Strain Y	L_{fx} [mm]	Strain X
LP	3661.37	16.59	0.1	21.01	0.01
HP	3560.75	18.71		21.15	

4. CONCLUSION

Based on the obtained results for give types of lattice structures were designed with different pore shapes, with ellipsoidal, X-shaped, helical, trapezoidal, and triangular cell units, the following conclusions were drawn.

- The surface quality of the printed lattice structures was examined using a digital microscope, revealing the presence of occasional un-sintered powder particles between the lattice struts. These anomalies have a negligible impact on compression test results.
- The tests revealed characteristic stress-strain curves, with apparent porosities ranging from 50.46% to 82%, surpassing the theoretical values obtained from CAD modeling, except for the helical structure.
- The apparent density and porosity of the structures varied across different designs, with the X-shape LP variant exhibiting the highest density (1.03 g/mm^3) and the HP trapezoidal variant having the lowest apparent density (0.647 g/mm^3).
- Detailed analyses of compression behavior involved distinguishing between monotonic and non-monotonic stress-strain curves. Apparent stress values at 5% and 15% apparent strain were normalized by the density of each sample. The helical structure, particularly in the LP variant, exhibited the highest force for 5% deformation, 16.49 kN/(g/mm^3), while X-shape LP demonstrated the highest force for 15% deformation, 22.08 kN/(g/mm^3).
- Initial stiffness values revealed a general decline with increasing porosity across all specimens. Notably, the helical LP variant displayed the highest initial stiffness (2395.3 1/g/mm^3). Comparative analyses of normalized forces for 15% deformation highlighted similarities between porous X-shape and trapezoidal structures.
- It has been shown that porous structure consisting of cell units with a helix structure has the most favorable mechanical properties. From this end, geometry of the designed structures is the main determinant of their mechanical properties in terms of the resistance to compression force.
- Finally, helical structure is characterized by the highest resistance to compression. To elucidate this, a comprehensive numerical analysis of this finding is extensively investigated in Part II.

As a summary of the study, it can be noted that the results indicate a high potential for purpose-designed porous structures to meet the requirements of certain applications in areas that require low-weight, high-stiffness such as biomedical and aerospace.

REFERENCES

1. Ruiz de Galarreta S, Jeffers JRT, Ghouse S. A validated finite element analysis procedure for porous structures. Mater Des. 2020 Apr 1;189:108546.
2. Guerra Silva R, Torres MJ, Zahr Viñuela J. A Comparison of Miniature Lattice Structures Produced by Material Extrusion and Vat Photopolymerization Additive Manufacturing. Polymers (Basel) [Internet]. 2021 Jul 1 [cited 2023 Jan 30];13(13). Available from: https://pubmed.ncbi.nlm.nih.gov/34208960/
3. Cipriani CE, Ha T, Martinez Defilló OB, Myneni M, Wang Y, Benjamin CC, et al. Structure–Processing–Property Relationships of 3D Printed Porous Polymeric Materials. ACS Mater Au. 2021 Sep 8;1(1): 69–80.
4. Chen H, Han Q, Wang C, Liu Y, Chen B, Wang J. Porous Scaffold Design for Additive Manufacturing in Orthopedics: A Review. Front Bioeng Biotechnol. 2020 Jun 17;8:609.
5. Tofail SAM, Koumoulos EP, Bandyopadhyay A, Bose S, O'Donoghue L, Charitidis C. Additive manufacturing: scientific and technological challenges, market uptake and opportunities. Mater Today. 2018 Jan 1;21(1):22–37.

6. Gadomska-Gajadhur A, Łojek K, Szymaniak M, Gadomska A. Materiały porowate do regeneracji tkanki chrzęstnej i kostnej. Wyr Med. 2018;3.
7. Kruk A, Gadomska-Gajadhur A, Ruskowski P, Chwojnowski A, Synoradzki L. Otrzymywanie polilaktydowych rusztowań komórkowych o strukturze gąbczastej – badania wstępne i optymalizacja procesu. Polimery. T. 62. 2017;2(2):118–26.
8. Mierzejewska Ż. Technologia SLS – charakterystyka i zastosowanie selektywnego spiekania laserowego w inżynierii biomedycznej. J Technol Exploit Mech Eng. 2015;1:178–90.
9. Maconachie T, Leary M, Lozanovski B, Zhang X, Qian M, Faruque O, et al. SLM lattice structures: Properties, performance, applications and challenges. Mater Des [Internet]. 2019 Dec 1 [cited 2023 Jun 16];183(10):108137. Available from: https://dx.doi.org/10.1115/1.4037305
10. Maconachie T, Leary M, Lozanovski B, Zhang X, Qian M, Faruque O, et al. SLM lattice structures: Properties, performance, applications and challenges. Mater Des [Internet]. 2019;183:108137. Available from: https://doi.org/10.1016/j.matdes.2019.108137
11. Uribe-Lam E, Treviño-Quintanilla CD, Cuan-Urquizo E, Olvera-Silva O. Use of additive manufacturing for the fabrication of cellular and lattice materials: a review. https://doi.org/101080/1042691420201819544 [Internet]. 2020 [cited 2023 Jun 16];36(3):257–80. Available from: https://www.tandfonline.com/doi/abs/10.1080/10426914.2020.1819544
12. Tao W, Leu MC. Design of lattice structure for additive manufacturing. Int Symp Flex Autom ISFA 2016. 2016 Dec 16;325–32.
13. Bhat C, Kumar A, Lin SC, Jeng JY. Design, fabrication, and properties evaluation of novel nested lattice structures. Addit Manuf. 2023 Apr 25;68:103510.
14. Kantaros A, Piromalis D. Fabricating Lattice Structures via 3D Printing: The Case of Porous Bio-Engineered Scaffolds. Appl Mech 2021, Vol 2, Pages 289-302 [Internet]. 2021 May 25 [cited 2023 Jun 16];2(2):289–302. Available from: https://www.mdpi.com/2673-3161/2/2/18/htm
15. Yuan S, Li S, Zhu J, Tang Y. Additive manufacturing of polymeric composites from material processing to structural design. Compos Part B Eng [Internet]. 2021;219(April):108903. Available from: https://doi.org/10.1016/j.compositesb.2021.108903
16. Hossain U, Ghouse S, Nai K, Jeffers JR. Controlling and testing anisotropy in additively manufactured stochastic structures. Addit Manuf. 2021 Mar 1;39:101849.
17. Pan C, Han Y, Lu J. Design and Optimization of Lattice Structures: A Review. Appl Sci 2020, Vol 10, Page 6374 [Internet]. 2020 Sep 13 [cited 2023 Jun 16];10(18):6374. Available from: https://www.mdpi.com/2076-3417/10/18/6374/htm
18. Wang P;, Yang F;, Zhao J, Wang P, Yang F, Zhao J. Compression Behaviors and Mechanical Properties of Modified Face-Centered Cubic Lattice Structures under Quasi-Static and High-Speed Loading. Mater 2022, Vol 15, Page 1949 [Internet]. 2022 Mar 6 [cited 2022 Aug 5];15(5):1949. Available from: https://www.mdpi.com/1996-1944/15/5/1949/htm
19. Beloshenko V, Beygelzimer Y, Chishko V, Savchenko B, Sova N, Verbylo D, et al. Mechanical Properties of Thermoplastic Polyurethane-Based Three-Dimensional-Printed Lattice Structures: Role of Build Orientation, Loading Direction, and Filler. 3D Print Addit Manuf [Internet]. 2021 May 14 [cited 2021 Nov 4];3dp.2021.0031. Available from: https://www.liebertpub.com/doi/abs/10.1089/3dp.2021.0031
20. Li S, Yuan S, Zhu J, Zhang W, Tang Y, Wang C, et al. Optimal and adaptive lattice design considering process-induced material anisotropy and geometric inaccuracy for additive manufacturing. Struct Multidiscip Optim. 2022 Jan 1;65(1):1–16.
21. Song J, Wang Y, Zhou W, Fan R, Yu B, Lu Y, et al. Topology optimization-guided lattice composites and their mechanical characterizations. Compos Part B Eng. 2019 Mar 1;160:402–11.
22. Bahrami Babamiri B, Askari H, Hazeli K. Deformation mechanisms and post-yielding behavior of additively manufactured lattice structures. Mater Des. 2020 Mar 1;188.
23. Yavas D, Liu Q, Zhang Z, Wu D. Design and fabrication of architected multi-material lattices with tunable stiffness, strength, and energy absorption. Mater Des [Internet]. 2022 May 1 [cited 2022 Nov 3];217:110613. Available from: https://linkinghub.elsevier.com/retrieve/pii/S0264127522002349
24. Yang L, Yan C, Cao W, Liu Z, Song B, Wen S, et al. Compression–compression fatigue behaviour of gyroid-type triply periodic minimal surface porous structures fabricated by selective laser melting. Acta Mater. 2019 Dec 1;181:49–66.
25. Park JH, Park K. Compressive behavior of soft lattice structures and their application to functional compliance control. Addit Manuf. 2020 May 1;33:101148.
26. Zhang L, Lifton J, Hu Z, Hong R, Feih S. Influence of geometric defects on the compression behaviour of thin shell lattices fabricated by micro laser powder bed fusion. Addit Manuf [Internet]. 2022 Oct 1 [cited 2022 Dec 20];58:103038. Available from: https://linkinghub.elsevier.com/retrieve/pii/S2214860422004304
27. Zhao Z, Wu Z, Yao D, Wei Y, Li J. Mechanical properties and failure mechanisms of polyamide 12 gradient scaffolds developed with selective laser sintering. J Mech Behav Biomed Mater. 2023 Jul 1;143:105915.
28. Han C, Li Y, Wang Q, Wen S, Wei Q, Yan C, et al. Continuous functionally graded porous titanium scaffolds manufactured by selective laser melting for bone implants. J Mech Behav Biomed Mater. 2018 Apr 1;80:119–27.

The author would like to express their sincere gratitude to Professor Krzysztof J. Kurzydłowski for his invaluable supervision and guidance throughout this study. Additionally, the author extends their thanks to Technology Applied Sp. z o. o for their generous support.

Monika Bernacka: https://orcid.org/0000-0003-3481-0768
Mehmet Aladag: https://orcid.org/0000-0002-2484-7519
Adrian Dubicki: https://orcid.org/0000-0002-3994-2957
Izabela Zglobicka: https://orcid.org/0000-0002-4432-9196